ACS APPLIED NANO MATERIALS

www.acsanm.org Article

Reversible Al Propagation in Si_xGe_{1-x} Nanowires: Implications for Electrical Contact Formation

Minh Anh Luong,* Eric Robin, Nicolas Pauc, Pascal Gentile, Thierry Baron, Bassem Salem, Masiar Sistani, Alois Lugstein, Maria Spies, Bruno Fernandez, and Martien den Hertog

Cite This: *ACS Appl. Nano Mater.* 2020, 3, 10427−10436 Read Online

ACCESS | Metrics & More | Article Recommendations | Supporting Information

ABSTRACT: While reversibility is a fundamental concept in thermodynamics, most reactions are not readily reversible, especially in solid-state physics. For example, thermal diffusion is a widely known concept, used among others to inject dopants into the substitutional positions in the matrix and improve device properties. Typically, such a diffusion process will create a concentration gradient extending over increasingly large regions, without possibility to reverse this effect. On the other hand, while the bottom-up growth of semiconducting nanowires is interesting, it can still be difficult to fabricate axial heterostructures with high control. In this paper, we report a thermally assisted partially reversible thermal diffusion process occurring in the solid-state reaction between an Al metal pad and a Si_xGe_{1-x} alloy nanowire observed by in situ transmission electron microscopy. The thermally assisted reaction results in the creation of a Si-rich region sandwiched between the reacted Al and unreacted Si_xGe_{1-x} part, forming an axial Al/Si/Si_xGe_{1-x} heterostructure. Upon heating or (slow) cooling, the Al metal can repeatably move in and out of the Si_xGe_{1-x} alloy nanowire while maintaining the rodlike geometry and crystallinity, allowing to fabricate and contact nanowire heterostructures in a reversible way in a single process step, compatible with current Si-based technology. This interesting system is promising for various applications, such as phase change memories in an all crystalline system with integrated contacts as well as Si/Si_xGe_{1-x}/Si heterostructures for near-infrared sensing applications.

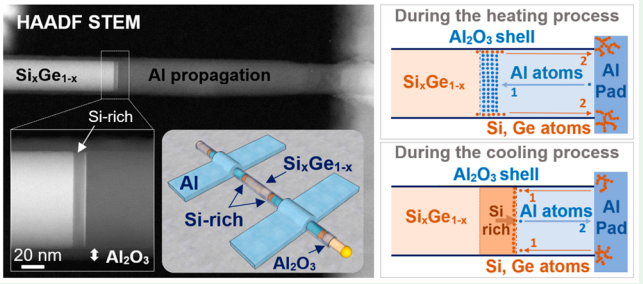

KEYWORDS: *Si/Si_xGe_{1-x} heterostructure, in situ transmission electron microscopy, nitride membrane, solid-state exchange reaction, solidification*

INTRODUCTION

Group IV semiconducting nanowires (NWs) are widely studied both by top-down and bottom-up approaches.[1,2] However, fabricating and contacting complex heterostructures with well-defined interfaces and contacts is still challenging, for example, because of the reservoir effect of the catalyst particle for bottom-up grown NWs.[3−6] Moreover contacting of NWs is likewise still challenging. Several papers have shown that a metal propagation in the NW can be used to form an intermetallic phase with a very abrupt contact with the original NW.[7−10] Having the metal contact inside the NW geometry has the additional advantage that the contacts do not screen the remaining semiconducting region from the gate,[11] as is the case with large metal contacts.

The diffusion behavior of Si/Al and Ge/Al binary systems in bulk and thin film materials has been studied for a long period, resulting in a large number of publications. In the Si/Al couple, because of the low solubility limit of Si in Al (about 1.62%),[12] the formed phase diagram shows a simple eutectic at 577 °C. Meanwhile, there is no report of metastable intermetallic compounds or glassy alloys in this binary system. It has been known that, above its solubility limit, Si would precipitate in particles or grains formed in the Al matrix.[13] On the other hand, Ge shows a higher solubility limit in Al with about 2% at a lower eutectic temperature of 420 °C. The diffusion coefficient of Ge in Al is higher than that of Si in Al at temperatures between room temperature and 600 °C,[14] the investigated temperature range in this study. In a nanowire system, the understanding of the diffusion behavior and kinetics of this ternary system is limited. As the ratio of surface area to the volume fraction increases, the surface energy could become a dominant factor. Consequently, the diffusion process would behave differently from bulk and thin film structures. In fact, because of the low solubility limits of Si in Al, and vice versa, there is no report of Al thermal diffusion in Si NWs, while Al can easily diffuse in Ge NWs at low temperature (<300 °C). This thermal diffusion process leads to the

Received: August 26, 2020
Accepted: September 16, 2020
Published: September 29, 2020

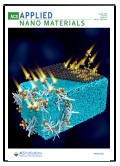

https://dx.doi.org/10.1021/acsanm.0c02303
ACS Appl. Nano Mater. 2020, 3, 10427−10436

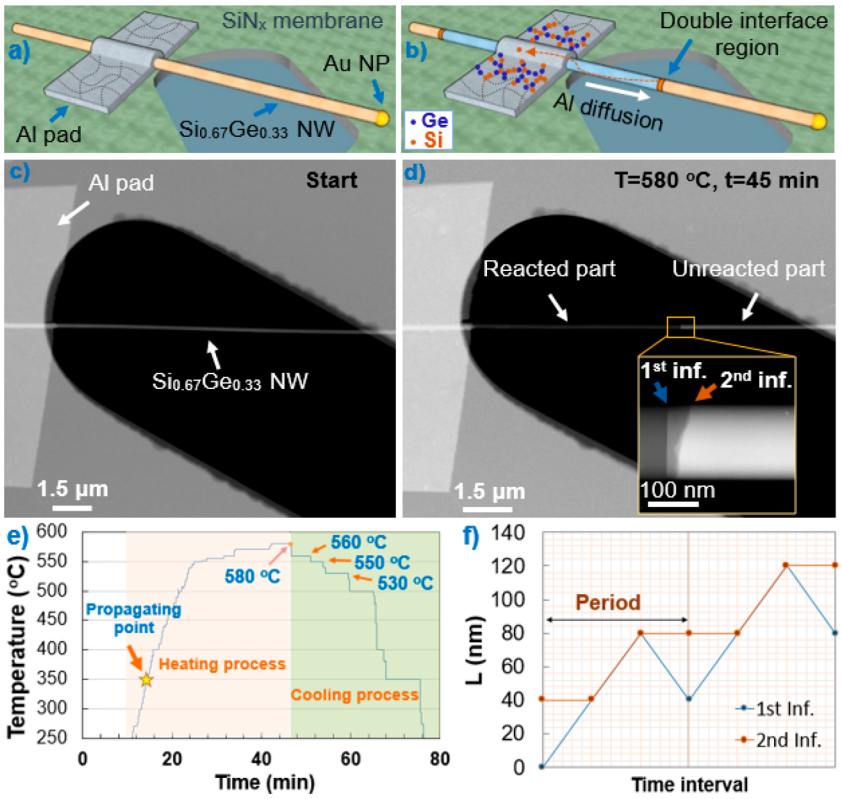

Figure 1. Real time observation of the thermal exchange between Al pads and a $Si_{0.67}Ge_{0.33}$NW during the heating process. (a, b) Schematic illustrations of the contacted NW before and after annealing for 45 min. Si and Ge atoms are displayed in orange and blue colors, respectively. The white arrow in (b) shows the propagating direction of the reaction interface while the orange arrow shows the diffusion of Si and Ge atoms in the opposite direction. (c, d) HAADF STEM images of the Al contacted $Si_{0.67}Ge_{0.33}$ NW crossing over the 6 μm × 23 μm hole of a SiN_x membrane before and after the in situ heating experiment. The diameter of the contacted NW is about 150 nm with a length of 20 μm. The inset in (d) shows the presence of a double-interface region, sandwiched between the Al reacted part and unreacted $Si_{0.67}Ge_{0.33}$ part. The abbreviation "Inf." refers to the interface. (e) Temperature profile as a function of time during the heating and cooling process. (f) Illustration of the relative positions of the first and second interface (Inf.) during the in situ heating. The video of this Al/$Si_{0.67}Ge_{0.33}$ propagation experiment is presented in Movie M1.

formation of a monocrystalline c-Al phase with an abrupt interface to the original Ge part, and no intermediate phase is formed. The real time observation and diffusion kinetics of Al/Ge thermal exchange have been described in detail in the work of Luong et al.[15,16] and El Hajraoui et al.,[17] where they propose that the rate of the thermal induced exchange reaction between the initial Ge NW and the Al is limited by Al volume diffusion, while Ge travels back into the Al metal contact by a surface diffusion mechanism. This interesting thermal diffusion process can be explained by the difference in diffusion coefficients, and we speculate that the driving force of the process is the fact that Ge can lower its energy by diffusing on a surface or grain boundary in Al metal when the system is heated. Additionally it was shown by Sistani et al.[18] that the selective propagation of Al in Ge−Si core−shell NWs created a radial heterostructure with a thin Si shell from the original NW wrapped around the Al/Ge/Al axial heterostructure.

In this paper, we report in situ transmission electron microscopy (TEM) observations of a thermally assisted solid-state exchange process between an Al metal pad and a Si_xGe_{1-x} alloy nanowire where we observe a partially reversible diffusion process, allowing to fabricate axial heterostructures starting from an initial homogeneous alloy NW. On heating, a reaction interface progresses in the NW where the Al metal replaces the original Si_xGe_{1-x} NW. On controlled cooling, a Si-rich region is progressively extending backward inside the just converted Al NW section, going from the interface with the original NW toward the Al contact pad. The crystallographic and compositional analyses on the created NW heterostructures are performed by using geometrical phase analysis (GPA)[19,20] and energy dispersive X-ray spectroscopy (EDX). 3D quantitative chemical reconstructions[21] of the heterostructure are presented to determine the distribution of chemical elements after the reaction process. We also present the result of the thermal reaction in passivated Si_xGe_{1-x}NWs with a 20 nm Al_2O_3 shell, demonstrating a significant improvement of the interface quality. From the ex situ and in situ observations, we propose a model to understand the formation of the Si/Si_xGe_{1-x} NW heterostructure. A large electrical resistance difference is observed with or without the Si-rich region, comparable to phase change materials (PCM) in memory devices.[22,23] Additionally, the created Si/Si_xGe_{1-x}/Si NW heterostructure is also promising for near-infrared sensing applications.[24−26]

IN SITU TEM OBSERVATION OF Al/$Si_{0.67}Ge_{0.33}$NW THERMAL EXCHANGE REACTION

In this study, as-grown NWs were dispersed on TEM temperature-calibrated heater chips, aiming for a direct observation of the Al metal protruding in $Si_{0.67}Ge_{0.33}$NWs. Figure 1c shows the high-angle annular dark-field (HAADF) scanning TEM (STEM) image of an Al contacted $Si_{0.67}Ge_{0.33}$NW lying over a hole before the annealing process, as schematically illustrated in Figure 1a. The NW diameter is

https://dx.doi.org/10.1021/acsanm.0c02303
ACS Appl. Nano Mater. 2020, 3, 10427−10436

about 150 nm with a length of 20 μm. The NW was contacted by a 200 nm thick Al rectangular pad, and the heating experiment was conducted inside the TEM microscope. To better describe the diffusion behavior, we will discuss the in situ experiment in two separate processes, i.e., (i) during the increase of the temperature when the temperature was slowly raised from room temperature to 580 °C (just above the eutectic temperature of Al/Si (577 °C)) with steps of 10 °C and (ii) during the controlled cooling to room temperature where the temperature was kept constant at 560, 550, and 530 °C for observation. The temperature profile of the entire experiment including (i) highlighted in pink color, and (ii) in green, is shown in Figure 1e.

i. During the Heating Process. Figure 1c shows the contacted $Si_{0.67}Ge_{0.33}$NW at the start of the experiment. When the temperature was increased following the temperature profile of Figure 1e, the HAADF-STEM contrast indicated initiation of the thermal exchange reaction starting at 350 °C where a darker contrast associated with the Al metal starts to enter the $Si_{0.67}Ge_{0.33}$NW through the NW surface underneath the Al contact pad. During the progression of the reaction interface, a series of HAADF STEM images were taken with 0.787 s per frame to follow the diffusion behavior, presented in Movie M1. Figure 1d shows the HAADF STEM image of the propagated NW when the heating temperature reached 580 °C after 45 min, as schematically represented in Figure 1b. The HAADF intensity is related to both the sample thickness and the mean atomic number of the elements. Because the $Si_{0.67}Ge_{0.33}$ alloy density is heavier than that of Al, the brighter contrast corresponds to the initial $Si_{0.67}Ge_{0.33}$NW and the darker contrast to the entering Al metal. While the NW diameter is reduced slightly in the reacted region (from 150 to 146 nm), this reduction alone could not account for the strong HAADF contrast (see the inset of Figure 1d). As indicated in Figure 1d, the "Reacted part" is the intrusion length of Al into the alloy NW of about 6.4 μm from the edge of the left Al contact pad. The inset in Figure 1d shows a zoom of the reaction interface, which surprisingly demonstrates the presence of an intermediate contrast region between the original $Si_{0.67}Ge_{0.33}$NW on the right and the reacted region on the left, termed the double-interface region. For convenience, the left interface between the Al-reacted part and double-interface region is called the first interface, and the one on the right between the double-interface region and unreacted $Si_{0.67}Ge_{0.33}$NW is called the second interface. The schematic illustrations of the contacted NW before and after annealing for 45 min are presented in Figure 1a,b. The white arrow shows the direction of Al thermal diffusion during the heating process, and the orange segment demonstrates the formation of the double-interface region. Prior to this study, we had observed the double-interface region in ex situ heating experiments. We speculated that the advancing Al would push the Si atoms ahead of the interface, gradually creating a larger and larger double-interface region. However, the in situ observation presented in Movie M1 is not at all compatible with this hypothesis and exhibits an entirely different process: the two interfaces show a violent kinetic behavior along the NW growth direction during the increase of the temperature. The plot in Figure 1f demonstrates the relative positions of the two interfaces during the heating. It can be observed that the interfaces do not advance smoothly, but rather advance in sub-50 nm sized steps, which can be as large as tens of nanometers. Because of the random behavior of the interface jumps, the time axis is not linear but adapted to show the forward and backward movement of the first interface. A careful analysis of the in situ experiment (Movie M1) reveals that the two interfaces are halted at the same position along the NW and that the two interfaces can momentarily catch up to be a single interface. Suddenly, the first interface then moves backward to generate a new double-interface segment along the NW axial direction, while the second interface can only halt or advance along the NW axis. The exchange reaction proceeds in this way and halts after a certain time when the temperature is constant. Then, the exchange reaction can be continued by increasing the temperature.

ii. During the Cooling Process. When the reaction interface had extended from the left to the right over a distance of 6.4 μm (at 580 °C), the heating temperature was slowly reduced to room temperature. At some points (i.e., 560, 550, and 530 °C), the temperature was kept constant to investigate the evolution of the reaction interfaces (see Figure 1e). Interestingly, the first interface was observed to extend in the reverse direction toward the left Al contact pad. Figure 2a shows the HAADF-STEM image of the propagated NW at 560 °C during the cooling process. The inset shows a HR-STEM image with the corresponding Fourier transform (FT) on the [011] zone axis (taken at the yellow box), which indicates the presence of twin structure defects starting from the NW surface and running across the NW diameter along the $[1\bar{1}1]$ direction.

Figure 2b shows the linear position dependence on time of the first interface diffusion length (L) in the reverse direction at three investigated temperatures (see legend to Figure 2b). It can be observed in Figure 2b that the reverse reaction rate accelerates at lower temperatures as the steepest slope is observed for the lowest temperature of 530 °C, indicating that the reverse reaction is driven by the reduction of the temperature. The in situ video of the reverse reaction of the first interface (at 560 °C) is presented in Movie M2. The second interface was carefully investigated showing no modification in shape and position. When the first interface had extended over a distance of 4.7 μm back toward the left Al contact pad, there was an enhancement of the HAADF intensity in the reverse reacted region until the reaction interface reached the Al contact pad, where a large crystal was then formed on the Al reservoir (see Figure 2c). Because the diameter of the reverse reacted region is constant, the observed increase in contrast is likely related to an increasing Ge content. The in situ video of the backward diffusion with the increase of the HAADF intensity is presented in Movie M3 (at 500 °C). EDX mapping acquired on the created crystal (Figure 2d) shows the main contribution of Ge in the crystal composition. The Si signal appears very weak and could be an artifact due to the scattered X-rays from the Si_3N_4 membrane. Figure 2e,f shows the schematic illustrations for the backward diffusion of first Si and later Ge atoms during the cooling process. Si atoms, being solute in the Al contact pad after the heating procedure, return to the NW during the cooling and fill the NW volume pushing the first interface in the reverse direction (Figure 2e), which is then followed by Ge atoms (Figure 2f).

STRUCTURAL AND COMPOSITIONAL ANALYSIS OF CREATED HETEROSTRUCTURES

To understand the mechanism of the exchange reaction, it is necessary to characterize the distribution of elements within

https://dx.doi.org/10.1021/acsanm.0c02303
ACS Appl. Nano Mater. 2020, 3, 10427−10436

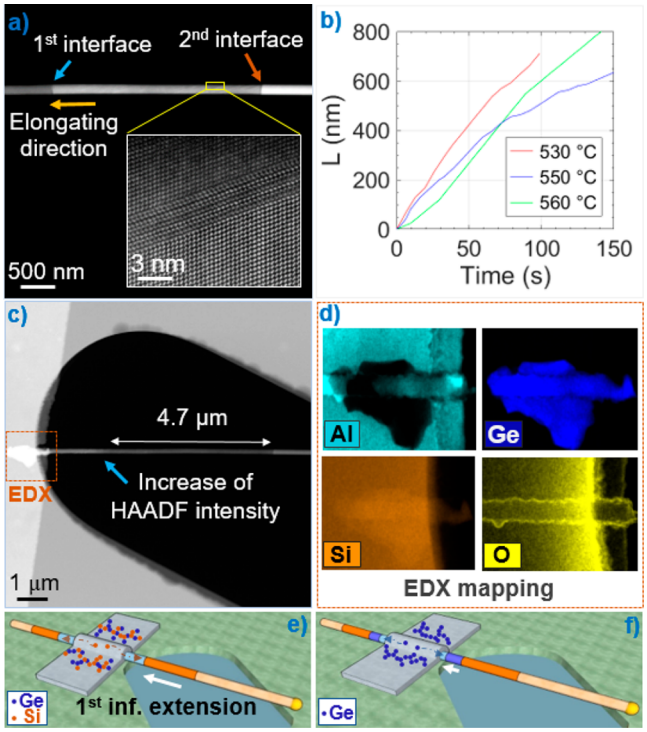

Figure 2. Real time observation of the thermal exchange between Al pads and a $Si_{0.67}Ge_{0.33}$NW during the cooling process. (a) HAADF-STEM image of a NW propagated at 560 °C during the cooling process, showing the movement of the first interface in the reverse direction toward the Al contact pad. The inset shows the zoom on the rectangular yellow box, demonstrating the formation of crystal defects in the newly formed NW region. (b) Plot of the first interface diffusion length (L) in reverse direction as a function of time at three different cooling temperatures, showing a linear diffusion behavior. (c) HAADF STEM image after 4.7 μm of backward propagation where an increase of HAADF intensity is observed in the created region as well as the formation of a large crystal when the first interface reached the Al contact pad. (d) EDX mapping on the created large crystal (indicated by the orange dashed box) at the Al contact pad showing the main contribution of Ge in the crystal composition. The in situ videos of the first interface during the cooling process (at 560 and 500 °C) are presented in Movie M2 and Movie M3, respectively. (e, f) Schematic illustrations of the propagated NW during the cooling process, showing the backward diffusion of both Si and Ge atoms.

the created structure. For these analyses, geometrical phase analysis (GPA) and quantitative EDX with a 3D reconstruction on different reacted parts were performed. To have a better statistic of created heterostructures for these experiments, as-grown $Si_{0.67}Ge_{0.33}$NWs were contacted on 200 nm thick Si_3N_4 membrane with holes and annealed ex situ via RTA at 400 °C for 20 s and then rapidly cooled to room temperature for 4 min. The HAADF STEM image of a contacted NW crossing over a 2 μm × 8 μm hole after the thermal treatment is presented in Figure S1a. Analysis of the lattice spacing using GPA indicated that the formed segment with intermediate contrast between the created Al part and original $Si_{0.67}Ge_{0.33}$ NW contains mostly Si. To obtain more precise chemical characterization, Figure 3 shows EDX quantification on each region of the created heterostructure (indicated by the dashed yellow box in Figure S1b). The distribution of Al, Si, Ge, and O elements are displayed in turquoise, orange, blue, and yellow, respectively. Figure 3a presents a line scan crossing the double-interface region from the Al reacted part to the unreacted $Si_{0.67}Ge_{0.33}$ part. The normalized concentration profile in atomic percent (at. %) was extracted by using QUANTAX-800 software from BRUKER, showing a transition from an Al part to a Si-rich region and then the $Si_{0.67}Ge_{0.33}$ original part. It is apparent that the double-interface region is mainly made of Si atoms. In addition, we observe a small gradient of Ge concentration from the first interface to the second interface, which is coherent with the HAADF intensity variation found in Figure S1b. The 3D reconstructions of the NW cross section on each particular region (using the modeling method from ref 21) are presented in Figure 3b–d. More details on the 3D reconstruction process are described in Figure S2. Figure 3b presents the mapping, radial line profile, and 3D reconstruction of the original $Si_{0.67}Ge_{0.33}$ NW. First, the radial profile demonstrates the presence of a homogeneous $Si_{0.67}Ge_{0.33}$ core, which is then covered by an oxide shell. Quantitatively, the as-grown NW has a $Si_{0.67}Ge_{0.33}$ core with the asymmetric diagonals of 74.3 and 65.4 nm. It is covered by 0.5 nm of thin Ge-rich shell (~43%) and 1 nm SiO_2 shell. EDX quantification for the Si-rich region is shown in Figure 3c. In the core part, there is an enrichment of the Si concentration with respect to the original part (67% Si) up to ≥90%. This region is also composed of small proportions of 5–6% Ge and 0–2% Al. It should be noted that the finding of ~2% Al in the core can be an artifact due to scattered X-rays of Al from the large Al contact pads. The outer shells are composed of a thin shell (about 1 nm) containing some Ge (8%) and then a mixture of Al_2O_3 and SiO_2 shell of about 2 nm. The presence of Al atoms in the shell parts can be attributed to the hypothesis that the Al reaction interface had reached the $Si_{0.67}Ge_{0.33}$ interface and then moved backward creating the Si-rich region (see also Movies M1–M3). Figure 3d shows the compositional analysis on the reacted part of the NW. The converted region has an Al core containing a noticeable 4% Si and small percent of Ge (about the quantification limit). In the literature,[12] the solubility limit of Si in Al is below 2%. Because the investigated region is near the Si_3N_4 membrane, a small contribution of Si X-rays scattered from the Si_3N_4 membrane is unavoidable, which will contribute to this quantification result. The outer shells consist of about 1 nm Ge containing shell and 1–2 nm of mixed Al_2O_3 and SiO_2 shell. It can be observed that the dimensions of especially the Si-rich and also the Al converted region are smaller than the original NW dimensions.

From the in situ observation of the Si-backward diffusion presented in Figure 2, it appeared that the cooling rate was the main parameter determining the extension length of the Si-rich segment. To confirm this prediction, we separated a similar set of fabricated Al contacted $Si_{0.67}Ge_{0.33}$ NWs into two parts and applied a thermal treatment (RTA) with two different recipes with a fast and slow cooling step, respectively. As can be seen in Figure S3, indeed the Si-rich segment length is much longer with a slow cooling step. This experiment interestingly demonstrates the possibility to tailor the $Si/Si_xGe_{1-x}/Si$ heterostructure size by controlling the temperature ramp during the heating and cooling process.

INFLUENCE of the Al_2O_3 PASSIVATION SHELL ON THE INTERFACE SHAPE

We have seen a clear influence of the NW diameter on the $Si_{0.67}Ge_{0.33}$ interface shape (see Figure S4). Particularly, small NWs with diameters ranging from 60 to 100 nm show the

https://dx.doi.org/10.1021/acsanm.0c02303
ACS Appl. Nano Mater. 2020, 3, 10427–10436

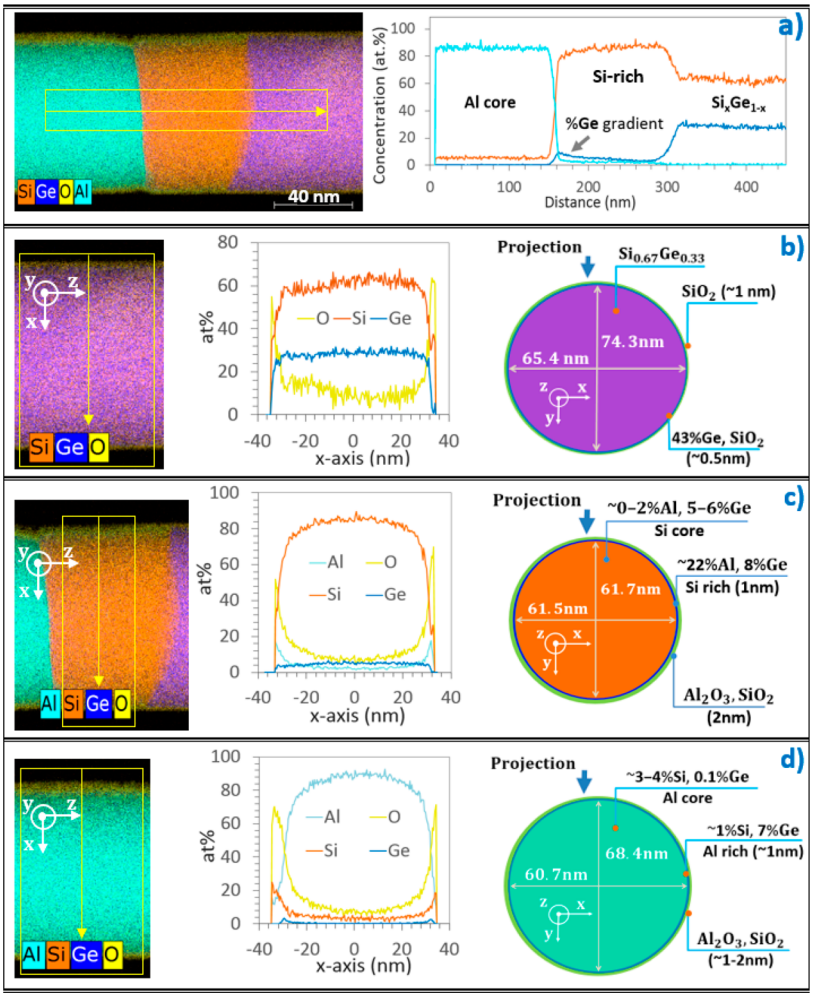

Figure 3. Compositional analysis on the created heterostructure using the quantitative energy dispersive X-ray spectroscopy technique. EDX mapping on the created heterostructures shown in Figure S1b (the dashed yellow box). (a) EDX hyper-map and line-scan profile crossing the heterostructures from the reacted, double-interface region and unreacted $Si_{0.67}Ge_{0.33}$ part. (b–d) EDX quantification on three different parts of the heterostructures, showing the chemical map, chemical profile, and 3D reconstruction, respectively. The vertical arrow indicates the projection direction of the elliptic reconstruction model

formation of a clean Si-rich/$Si_{0.67}Ge_{0.33}$ interface with a straight or more often observed, convex shape (Figure S4a). Larger NW diameters (150–250 nm), however, show the presence of a very rough interface with different facets (shown in Figure S4b).

From the in situ observation presented in Figure 1d, where it was observed that both interfaces move in relatively large steps and both interfaces halt at the same positions along the NW, we speculated that the interfaces can be trapped at specific surface locations, and therefore the formation of the interface shape will be strongly influenced by the surface quality. To verify this hypothesis, we cleaned the NW surface by hydriodic acid (HI) and immediately passivated the as-grown NWs with a 20 nm Al_2O_3 shell (using atomic layer deposition (ALD) at 250 °C). The NWs were then contacted on both ends with 200 nm thick Al pads and deposited on Si_3N_4 membranes and TEM calibrated heater chips for ex situ and in situ annealing experiments, respectively. For the ex situ heating experiment, the contacted NWs were annealed at 450 °C for 10 s and rapidly cooled to room temperature. Figure 4a shows the HAADF STEM image of a contacted 77 nm thick $Si_{0.67}Ge_{0.33}$NW with a 20 nm Al_2O_3 passivation shell after the thermal treatment, showing the Al conversion length of about 650 nm and Si-rich segment of 14 nm. Figure 4b shows the magnified image taken in the blue box in the inset of Figure 4a, showing the alignment of $Si_{0.67}Ge_{0.33}$ (111)//Si-rich (111)//Al (111) planes. Again, we can observe a brighter HAADF contrast between the Si-rich region and Al-reacted part (about five atomic planes), which is attributed to a locally increased Ge content.

We have also performed an in situ heating experiment in two coalesced and passivated $Si_{0.67}Ge_{0.33}$NWs (see Movie M4). As can be seen from the movie, the diffusion process was smoother and the $Si_{0.67}Ge_{0.33}$ interface appeared very sharp. Compared to the unpassivated NW (Figure 2a), the crystalline quality of the Si-rich region is improved, as no twin defects were observed in the passivated NWs. These results confirm the critical role of NW surface quality on the diffusion behavior and kinetics of the exchange reaction. Probably, the NW surface quality had been significantly improved after the NW surface cleaning by the wet etching process and the protection of the 20 nm Al_2O_3 passivation shell.

https://dx.doi.org/10.1021/acsanm.0c02303
ACS Appl. Nano Mater. 2020, 3, 10427–10436

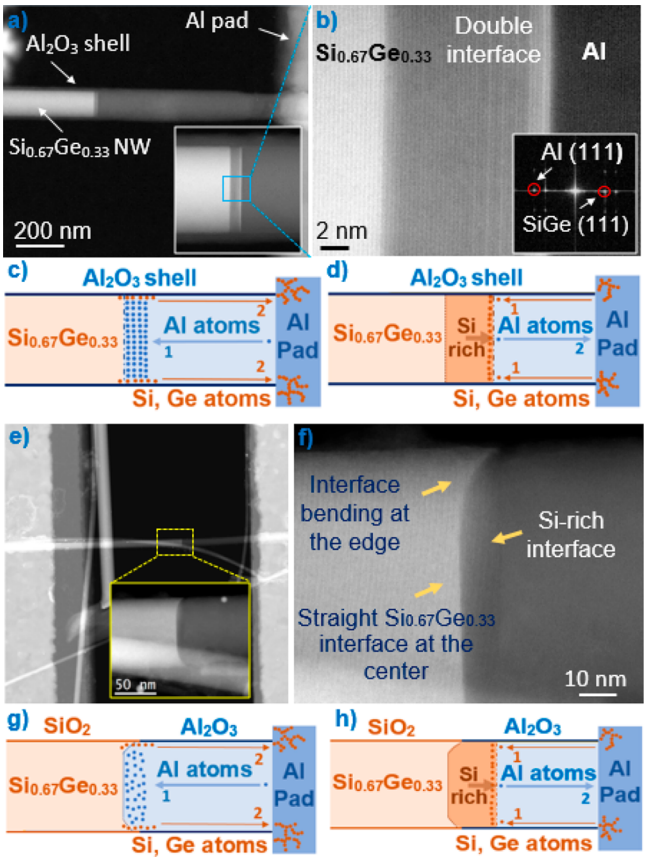

Figure 4. Interface shape for passivated and as-grown NWs and corresponding diffusion model. (a) HAADF STEM image of propagated NW passivated with 20 nm of Al_2O_3 showing the formation of Al/Si-rich/Si_xGe_{1-x} heterostructure. The contacted NW was annealed at 450 °C for 10 s and rapidly cooled to room temperature. (b) HR HAADF STEM image obtained at the blue box in the inset of (a), with the corresponding Fourier transform, showing an epitaxial alignment of Al/Si-rich and Si-rich/$Si_{0.67}Ge_{0.33}$ interfaces on the [111] reflection. Also see the in situ video of the Al thermal diffusion in passivated NWs shown in Movie M4 and Figure S5. (c, d) Schematic illustrations of the diffusion paths of Si, Ge, and Al atoms during the heating and cooling process, respectively. (e) HAADF-STEM image of Al contacted Si_xGe_{1-x}NW (83 nm in diameter) after being annealed at 400 °C for 20 s, 400 to 300 °C for 30 s, and cooled to room temperature for 4 min. The inset shows the zoom on the reaction interface having a convex shape. (f) Magnified image on the top part of the reaction interface showing a straight interface at the center and a bending shape at the NW edge. (g, h) Schematic illustrations of Al, Si, and Ge diffusion direction during the forward propagation of the Si_xGe_{1-x} interface and backward diffusion of the Si-rich interface, respectively.

TRANSPORT PROPERTIES THROUGH THE CREATED HETEROSTRUCTURES

For device applications, it is of crucial importance to investigate the electrical transport property of the created heterostructures. We have therefore performed electrical measurements on the $Si_{0.67}Ge_{0.33}$ NWs before and after the thermal diffusion. Figure S6a shows the BF STEM image of a contacted NW after the thermal reaction via RTA. The exchange reaction has taken place from two sides of the contacted NW (190 nm in diameter), leaving a remaining unreacted $Si_{0.67}Ge_{0.33}$ segment of about 1.75 μm. The plot in Figure S6b shows the IV characteristics of the contacted NW before and after the thermal propagation. First, we can see that the current passing through the undoped $Si_{0.67}Ge_{0.33}$ NW is very low, in the order of 10^{-10} A for a biasing voltage of 1 V. After the metal intrusion, the resistance has increased significantly so that the measured current dropped 2 orders of magnitude. The reacted Al metal part has a low resistance.[27] Therefore, in the case of this same process in pure Ge NWs, the resistance of the remaining Ge region will become smaller and smaller as its length is reduced, since it is resistivity will not change significantly. In the experiments with Al propagation in $Si_{0.67}Ge_{0.33}$ NWs, we observe the opposite effect: the NW becomes much more resistive, even when its total volume has become much smaller. Potentially, with the presence of the Si-rich region between the reacted and unreacted part, which has a large bandgap energy, the current is blocked by the band offset at the Si/$Si_{0.67}Ge_{0.33}$ interface, causing the drop of the measured current. The Si-rich region is potentially doped by Al since this region is created after it has already been converted to pure Al, when the first interface moves backward. However, the strong increase in resistance after Al has propagated in the NW does not indicate a high doping of the Si-rich region.

The possibility to modulate the resistance is promising for applications as phase change materials in an all-crystalline system, avoiding known challenges as chemical segregation.[28−30]

REPETITIOUS CYCLE PROPERTY

The diffusion behavior of this ternary system combined with the change in resistivity may be promising for phase change memory applications.[22,23] Therefore, we have tested the cyclability on an Al contacted unpassivated $Si_{0.67}Ge_{0.33}$ NW (having a diameter of 210 nm) by exposing it to alternating heating and cooling cycles around the eutectic temperature of Al/Si, as shown in Movie M5. Interestingly, it is possible to remove and reproduce the Si-rich segment for several cycles while maintaining the NW geometry and unreacted $Si_{0.67}Ge_{0.33}$ part. However, the Si-rich segment length appeared shorter after each cycle, which is attributed to loss of Si atoms which had moved out and had not returned to the NW. It is therefore necessary to optimize the temperature window during the cooling process to stabilize the number of returning Si atoms for a precise control of the Si-rich segment length.

DISCUSSION

Recalling the diffusion behavior shown in the Movie M1, the two interfaces moved forward catching up with each other after a certain time, and then the $Si_{0.67}Ge_{0.33}$ interface suddenly stopped while the Si-rich interface moved backward to generate a new Si-rich region. First, the stepwise propagation of the $Si_{0.67}Ge_{0.33}$ interface may be explained due to the presence of defects or roughness on the NW surface. Because as-grown NWs were exposed to air, the NW surface was strongly oxidized, resulting in the formation of surface defects. The EDX quantification has shown the presence of an about 1−2 nm thick SiO_2 shell around the NW. Therefore, the trapping and detrapping of the reaction interface at these defects may cause the discontinuous propagation of the $Si_{0.67}Ge_{0.33}$ interface and the presence of several facets. This hypothesis was corroborated by the formation of a clean and sharp $Si_{0.67}Ge_{0.33}$ interface when passivating the NWs by a 20 nm Al_2O_3 shell. Then, the Si-rich interface moved in the reverse direction after the $Si_{0.67}Ge_{0.33}$ interface had stopped.

https://dx.doi.org/10.1021/acsanm.0c02303
ACS Appl. Nano Mater. 2020, 3, 10427−10436

From Figure 3d, we observed about 4% of Si content in the Al reacted part (higher than the solubility limit of Si in Al, 1.64%[12]); this part may be saturated by Si atoms. The saturation of Si content in the diffusion channel results in the precipitation of Si at the $Si_{0.67}Ge_{0.33}$ interface, forming the Si-rich region in an in-equilibrium state. The Si-rich region then acts as a barrier layer preventing Ge atoms of the original $Si_{0.67}Ge_{0.33}$ part from moving toward the Al reservoir, and hence the $Si_{0.67}Ge_{0.33}$ interface is blocked during the presence of the Si-rich region. After a certain time, when the Si content in the diffusion channel (Al core and surface in the reacted part) drops below the solubility limit, the Si-rich segment disappears and the $Si_{0.67}Ge_{0.33}$ interface again starts a new cycle of propagation. It is also observed that there is a gradient of Ge content in the Si-rich region with a maximum of Ge at the Al/Si-rich interface. This may indicate that forming an interface between monocrystalline Al and Si is energetically not allowed at the experimentally accessible temperature. Therefore, to decrease the energy of the interface, the Ge content must increase at the Al interface. This would also explain why the exchange reaction was never observed in the Al/Si binary couple.

From the Movie M2, when the temperature was slowly reduced, the Si-rich interface was observed to move in the reverse direction toward the Al contact pad, consequently extending the Si-rich region. Because the interface with the original $Si_{0.67}Ge_{0.33}$NW did not show any change during extension of the Si-rich region, it is expected that Si atoms that previously moved out of the NW and into the grain boundaries or surface of the Al reservoir are now diffusing back and reconstitute the NW cross section. From the literature,[31−33] this phenomenon can be explained by the solidification process of the Al/Si binary system (with an eutectic temperature of 577 °C). The lowering of the temperature below the eutectic temperature leads to a considerable drop of the Si solubility in the Al reservoir, resulting in the precipitation of Si atoms. The unreacted $Si_{0.67}Ge_{0.33}$ part can be a reasonable nucleation point for an epitaxial precipitation due to the high Si content.

Diffusion is defined as the migration of matter down a concentration gradient. Therefore, in a situation where a metal diffuses into a NW, we typically expect to see an interdiffused region. On the other hand, in such experiments where a metal enters a NW (for example, with Ni in the case of Si or Ge NWs,[34,35] Cu in Ge NWs,[36,37] Pt in Si NWs,[38] or Al in Ge NWs[15,39]) a very abrupt interface is observed between the original NW and the converted region. The likely explanation is that the concentration gradient is not present along the NW axis but is present in a surface diffusion channel.[17,37] Considering these two points, we believe the observed reversible diffusion occurs like this:

- *Heating*: Al from the contact pad is supplied to the reaction interface by self-diffusion of Al through the volume of the already converted region (see blue arrows in the schematics of Figure 4c). Si and Ge diffuse away from the NW through a surface channel and incorporate at surfaces and grain boundaries of the Al contact pad (see orange arrows in the schematics of Figure 4c). Indeed, both Si and Ge are detected close to the surface of the converted part of the NW, as evidenced by chemical mapping in Figure 3d. The concentration gradient of Al would therefore be found in the Al volume and those of Si and Ge in a surface diffusion channel.
- *Cooling*: When the temperature is lowered, the capacity to store Si and Ge atoms at Al surfaces and grain boundaries is reduced. Therefore, these locations now become the high concentration locations. This can be regarded as a sponge full of water (hot Al pad full of Si and Ge atoms), which then is pressed: it can no longer contain all the water, so this water needs to go somewhere else (Si and Ge atoms need to diffuse somewhere else). Therefore, Si and Ge diffuse back into the NW through the surface channel, and Al diffuses back into the Al pad; all concentration gradients are now reversed with respect to the heating situation (Figure 4d). The driving force of the reversible reaction is a change in solubility with temperature of the Si/Ge in the Al surfaces and grain boundaries in the contact pad. The reversible reaction applies only to the created Si-rich region, since it is not possible to recreate the original $Si_{0.67}Ge_{0.33}$NW.

During the elongation of the Si-rich region, we have observed the shrinkage of the NW diameter that may occur due to the replacement of Ge atoms by Si atoms with smaller radius, making the crystal structure become more compact. Reduction of the NW diameter could also partly be explained by the fact that the NW volume does not necessarily have to be filled with Al or Si (and Ge) atoms exactly to the level it was prior to any reaction. After the backward diffusion of the Si atoms, we observed the increase of HAADF intensity evidencing returning Ge atoms, also demonstrated by the formation of a crystal on the Al pad when the retreating reaction interface reached the Al pad. From the EDX mapping of the crystal presented in Figure 2d we find that the crystal is mainly composed of Ge atoms. The Si signal at the Ge crystal appears very weak, which indicates an exhaustion of Si content in the Al contact reservoir. The backward diffusion of Ge atoms after the exhaustion of Si atoms is explained by the lower Al/Ge eutectic temperature (420 °C) compared to Al/Si (577 °C). The backward diffusion of Si followed by Ge atoms is a remarkably interesting phenomenon that has not been reported in the literature and has not been observed in the binary Al/Ge NW system.[17] These results demonstrate that the NW geometry guides the recrystallization of a supersaturated element (in this case Si and Ge) in a controllable and repeatable fashion, which may also apply to other material couples.

Unlike the diffusion behavior in large NW diameters (≥150 nm) resulting in the formation of a rough $Si_{0.67}Ge_{0.33}$ interface, the created $Si_{0.67}Ge_{0.33}$ interfaces in small NW diameters (≤100 nm) are typically clean with a convex shape. Figure 4e shows the HAADF STEM image of a propagated $Si_{0.67}Ge_{0.33}$NW lying over a hole on the Si_3N_4 membrane and a zoomed image on the reaction interface. Magnifying the top part of the reaction interface shown in Figure 4f, we can see a straight interface at the center and a bending shape when it comes to the interface edge. From this interface shape it is expected that the exchange reaction does not start from the surface but nucleates in the NW core and extends to the surface. This can be the reason the created interfaces are mostly abrupt and clean without any facet. Figure 4g,h presents the schematic illustrations of Al, Si, and Ge diffusion direction during the heating (g) and cooling (h) process. During the forward diffusion of the $Si_{0.67}Ge_{0.33}$ interface, Al atoms from the contact pad will move through the converted Al region to

https://dx.doi.org/10.1021/acsanm.0c02303
ACS Appl. Nano Mater. 2020, 3, 10427−10436

exchange with the Si and Ge atoms at the interface (path 1), starting from the center and spreading out toward the interface edge. From the results of the EDX quantification presented in Figure 3, in the unreacted $Si_{0.67}Ge_{0.33}$ part, Si and Ge surface atoms make bonds with oxygen atoms forming the stable SiO_2 shell (with a small fraction of GeO_2 shell since the Si/Ge ratio is ~0.67/0.33), whereas the freshly created Al part is oxidized, creating an Al_2O_3 shell. Considering the different bond dissociation energy (enthalpy) for Si−O (799.6 ± 13.4 kJ/mol) and Al−O (501.9 ± 10.6 kJ/mol),[40] the $SiO_2/Si_{0.67}Ge_{0.33}$ interface is more stable than the Al_2O_3/Al interface. Therefore, when approaching the NW surface, the exchange reaction is decelerated at the interface edge, causing the formation of a convex interface. A similar argument was raised in the paper of Chou et al.,[41] where they interpreted the formation of a convex interface between Si and Co. Figure 4 summarizes the interface shape and diffusion model for NWs with (Figure 4a−d) and without (Figure 4e−h) a 20 nm Al_2O_3 shell.

In the case of passivated NWs, because of the presence of the predeposited Al_2O_3 shell on both sides of the reaction interface, the interfacial energy difference between the unreacted segment ($Al_2O_3/Si_{0.67}Ge_{0.33}$) and reacted segment ($Al_2O_3$/Al) has been reduced. Therefore, the reaction rate is unaffected by the interfacial energy difference on both sides of the reaction interface, resulting in the formation of a flat $Si_{0.67}Ge_{0.33}$ interface (see Figure 4).

CONCLUSION

In summary, the Al−(Si, Ge) NW thermal exchange reaction was investigated in detail via ex situ and in situ heating techniques. The incorporation of Al metal in $Si_{0.67}Ge_{0.33}$ alloy NWs results in the formation of a Si-rich region (≥90%), sandwiched between the reacted and unreacted part of the NW. When reducing the heating temperature, we have observed a linear extension of the Si-rich segment length in the reverse direction back to the Al contact pad. In small NW diameters, the interfacial energy between the core and oxide shell on both sides of the reaction interface becomes more significant and governs the exchange reaction. A clean convex $Si_{0.67}Ge_{0.33}$ interface results from the deceleration of the diffusion rate from the center to the edge of the NW due to the lower interfacial energy of the $SiO_2/Si_{0.67}Ge_{0.33}$ interface compared to that of the Al_2O_3/Al interface. With a predeposited Al_2O_3 shell, the interfacial energies on both sides of the reaction interface are reduced significantly, which results in the formation of flat atomically abrupt $Si_{0.67}Ge_{0.33}$ and Si-rich interface and much smoother advancement of the reaction interface. Then, during the cooling process, the linear extension of the Si and Ge atoms is explained by the solidification process of the Al−(Si, Ge) ternary system. Slowly decreasing the temperature induces the precipitation of first Si and then Ge atoms, starting at the unreacted $Si_{0.67}Ge_{0.33}$ part. Current−voltage characteristics without (on-state) and with the presence of the Si/Si_xGe_{1-x}/Si heterostructure (off-state) show a current drop of 2 orders of magnitude ($I_{on}/I_{off} = 10^2$), respectively. This ratio is expected to be improved when employing doped Si_xGe_{1-x} alloy nanowires to raise the on-state current. In summary, these findings show the possibility to produce tunable Al/Si/Si_xGe_{1-x} axial heterostructures with integrated contacts, created in a single fabrication step. These structures may show a great potential for phase change memories as well as near-infrared (NIR) sensing applications since Si_xGe_{1-x} alloys show an interesting flexible bandgap that can be tuned in the 1.3−1.55 μm telecommunication window,[42,43] all in a system compatible with current silicon-based technology. Moreover, the observed reversible thermal diffusion of the metal, certainly due to the NW system confining semiconductor and metal in an oxidized shell, may be a concept that can be extended to other material couples.

METHODS

In this work, we have conducted the thermal diffusion of Al metal into three different Si_xGe_{1-x} alloy stoichiometries (i.e., x = 0.05, 0.12, and 0.67). However, for Al diffusion in low composition Si NWs (x = 0.05 and 0.12) no clear difference with the pure Ge NW system was observed, and a strikingly different behavior was observed in the NWs with x = 0.67. Therefore, we decided to focus on the Si_xGe_{1-x} NWs (x = 0.67) in our experiments. The growth of $Si_{0.67}Ge_{0.33}$NWs was performed by the chemical vapor deposition method (CVD) via the VLS growth mode using silane and GeH_4 gases as precursors and gold as catalyst on a Si(111) substrate. The NWs were grown along the [111] direction. The fabricated NWs have a strong variation in diameter, ranging from 60 to 250 nm. For the experiments, as-grown NWs were either being used directly to perform metal contacts or a surface passivation was applied by cleaning the NW surface by dipping in diluted hydriodic acid (HI) for 5 s and immediately passivating by a 20 nm Al_2O_3 shell (using atomic layer deposition at 250 °C). Aiming for in situ heating experiments, $Si_{0.67}Ge_{0.33}$NWs were dispersed on calibrated heater chips from DENSsolutions,[44] which contain several 6 μm × 23 μm holes on the SiN_x membrane and have the possibility to raise the temperature up to 1300 °C within a few seconds. We then selected NWs lying over the holes and contacted both sides by a pair of Al rectangular pads. Prior to the deposition of Al metal layer, NWs with the 20 nm Al_2O_3 shell were immersed in buffered hydrofluoric acid−BOE 7:1 ($HF:NH_4F$ = 12.5:87.5%) for 40 s to remove the Al_2O_3 shell in the contact regions and then dipped in diluted hydriodic acid (HI) for 5 s to etch the native GeO_2 shell. After that, the samples were cleaned by soft Ar plasma for 15 s and coated by a 200 nm Al thick layer using electron beam evaporation (with the purity of 99.995% and in a vacuum at a pressure lower than 10^{-6} Torr). The samples were lifted off in acetone solution overnight to obtain the final devices. For temperature calibrated in situ heating experiments, the samples were heated inside the TEM microscope by using a commercial DENSsolutions six-contact, double-tilt TEM heating holder. The in situ heating process started from room temperature, and the temperature was gradually increased with 10 °C steps until reaching 580 °C. We then slowly reduced the heating temperature and stopped at certain temperatures for observation. In this study, $Si_{0.67}Ge_{0.33}$NWs were also contacted on homemade 200 nm Si_3N_4 membranes for ex-situ heating experiments using rapid thermal annealing (RTA). The fabrication of the Si_3N_4 membranes is reported elsewhere.[45] For ex situ heating experiments, several contacted NWs can be propagated at the same condition, giving more statistics on the reaction behavior. To conduct the thermal exchange reaction, specimens were annealed in a temperature range of 400−450 °C in a N_2 atmosphere and rapidly or slowly cooled to room temperature. The RTA experiments were done in a Jipelec JetFirst RTP Furnace.[46] The data of crystallographic and compositional analysis were collected by using a FEI Titan Themis microscope equipped with a probe Cs corrector and SuperX EDX (4 SDDs) detectors working at 200 kV. High angle annular dark field (HAADF) scanning TEM (STEM) was performed with a beam convergence angle of 20.7 mrad and electron beam current of 96 pA.

ASSOCIATED CONTENT

Supporting Information

The Supporting Information is available free of charge at https://pubs.acs.org/doi/10.1021/acsanm.0c02303.

Figure S1: the structure analysis of the created heterostructures using geometrical phase analysis;

https://dx.doi.org/10.1021/acsanm.0c02303
ACS Appl. Nano Mater. 2020, 3, 10427−10436

Section S2: basic steps of the 3D reconstruction method; Figure S3: comparison of the Si-rich segment length (L) in propagated NWs with respect to two different cooling processes; Figure S4: influence of NW diameter on the $Si_{0.67}Ge_{0.33}$ interface shape; Figure S5: influence of the passivation shell on the formation of the $Si_{0.67}Ge_{0.33}$ interface shape; Figure S6: IV characteristics measured on the contacted NW before and after the thermal propagation (PDF)

Movie M1: in situ propagation of Al metal into a 150 nm $Si_{0.67}Ge_{0.33}$NW lying over a hole on the SiN_x membrane (calibrated heater chip from DENSsolutions) during the heating process (0.787 s per frame, accelerated 15 frames/s) (MP4)

Movie M2: backward diffusion of the first interface during the cooling process (at 560 °C) (0.787 s per frame, accelerated 15 frames/s) (MP4)

Movie M3: increase of the HAADF contrast and formation of a crystal when the first interface reaches the Al contact pad (at 500 °C) (0.787 s per frame, accelerated 10 frames/s) (MP4)

Movie M4: in situ observation of the exchange reaction on two passivated $Si_{0.67}Ge_{0.33}$NWs (0.787 s per frame, accelerated 15 frames/s) (MP4)

Movie M5: in situ propagation in an Al contacted unpassivated $Si_{0.67}Ge_{0.33}$ NW (having a diameter of 210 nm) during an alternating heating and cooling process around the eutectic temperature of Al/Si (0.787 s per frame, accelerated 25 frames/s) (MP4)

AUTHOR INFORMATION

Corresponding Author

Minh Anh Luong − *CEA-Grenoble, IRIG-DEPHY-MEM-LEMMA, Université Grenoble Alpes, F-38054 Grenoble, France;* orcid.org/0000-0002-0876-2400; Email: minhanhapc@gmail.com

Authors

Eric Robin − *CEA-Grenoble, IRIG-DEPHY-MEM-LEMMA, Université Grenoble Alpes, F-38054 Grenoble, France;* orcid.org/0000-0002-5596-2640

Nicolas Pauc − *CEA-Grenoble, IRIG-DEPHY-PHELIQS-SINAPS, Université Grenoble Alpes, F-38000 Grenoble, France*

Pascal Gentile − *CEA-Grenoble, IRIG-DEPHY-PHELIQS-SINAPS, Université Grenoble Alpes, F-38000 Grenoble, France;* orcid.org/0000-0002-1547-4247

Thierry Baron − *CNRS, LTM, Université Grenoble Alpes, 38054 Grenoble, France*

Bassem Salem − *CNRS, LTM, Université Grenoble Alpes, 38054 Grenoble, France;* orcid.org/0000-0001-8038-3205

Masiar Sistani − *Institute of Solid State Electronics, Technische Universität Wien, Vienna 1040, Austria;* orcid.org/0000-0001-5730-234X

Alois Lugstein − *Institute of Solid State Electronics, Technische Universität Wien, Vienna 1040, Austria;* orcid.org/0000-0001-5693-4775

Maria Spies − *CNRS, Institut NEEL UPR2940, Université Grenoble Alpes, Grenoble 38042, France;* orcid.org/0000-0002-3570-3422

Bruno Fernandez − *CNRS, Institut NEEL UPR2940, Université Grenoble Alpes, Grenoble 38042, France*

Martien den Hertog − *CNRS, Institut NEEL UPR2940, Université Grenoble Alpes, Grenoble 38042, France;* orcid.org/0000-0003-0781-9249

Complete contact information is available at: https://pubs.acs.org/10.1021/acsanm.0c02303

Notes

The authors declare no competing financial interest.

ACKNOWLEDGMENTS

We acknowledge support from the Laboratoire d'excellence LANEF in Grenoble (ANR-10-LABX-51-01). We benefitted from the access to the Nano characterization platform (PFNC) in CEA Minatec Grenoble and Nanofab from Institute NEEL, Grenoble. This project has received funding from the European Research Council (ERC) under the European Union's Horizon 2020 research and innovation programme (grant agreement no. 758385) for the e-See project. The authors gratefully acknowledge financial support by the Austrian Science Fund (FWF) (project no. P28175-N27).

ABBREVIATIONS

CVD, chemical vapor deposition; VLS, vapor−liquid−solid; NWs, nanowires; ALD, atomic layer deposition; STEM, scanning transmission electron microscope; RTA, rapid thermal annealing; HAADF, high-angle annular dark-field imaging; EDX, energy dispersive X-ray spectroscopy; GPA, geometric phase analysis; NIR, near-infrared; Inf., interface.

REFERENCES

(1) Hobbs, R. G.; Petkov, N.; Holmes, J. D. Semiconductor Nanowire Fabrication by Bottom-Up and Top-Down Paradigms. *Chem. Mater.* **2012**, *24* (11), 1975−1991.

(2) Cui, Y. Functional Nanoscale Electronic Devices Assembled Using Silicon Nanowire Building Blocks. *Science* **2001**, *291* (5505), 851−853.

(3) Li, N.; Tan, T. Y.; Gösele, U. Transition Region Width of Nanowire Hetero- and Pn-Junctions Grown Using Vapor−Liquid−Solid Processes. *Appl. Phys. A: Mater. Sci. Process.* **2008**, *90* (4), 591−596.

(4) Clark, T. E.; Nimmatoori, P.; Lew, K.-K.; Pan, L.; Redwing, J. M.; Dickey, E. C. Diameter Dependent Growth Rate and Interfacial Abruptness in Vapor−Liquid−Solid $Si/Si_{1-x}Ge_x$ Heterostructure Nanowires. *Nano Lett.* **2008**, *8* (4), 1246−1252.

(5) Perea, D. E.; Li, N.; Dickerson, R. M.; Misra, A.; Picraux, S. T. Controlling Heterojunction Abruptness in VLS-Grown Semiconductor Nanowires via in Situ Catalyst Alloying. *Nano Lett.* **2011**, *11* (8), 3117−3122.

(6) Periwal, P.; Sibirev, N. V.; Patriarche, G.; Salem, B.; Bassani, F.; Dubrovskii, V. G.; Baron, T. Composition-Dependent Interfacial Abruptness in Au-Catalyzed $Si_{1-x}Ge_x$ /$Si/Si_{1-x}Ge_x$ Nanowire Heterostructures. *Nano Lett.* **2014**, *14* (9), 5140−5147.

(7) Wu, Y.; Xiang, J.; Yang, C.; Lu, W.; Lieber, C. M. Single-Crystal Metallic Nanowires and Metal/Semiconductor Nanowire Heterostructures. *Nature* **2004**, *430* (6995), 61−65.

(8) Zwanenburg, F. A.; van Loon, A. A.; Steele, G. A.; van Rijmenam, C. E. W. M.; Balder, T.; Fang, Y.; Lieber, C. M.; Kouwenhoven, L. P. Ultrasmall Silicon Quantum Dots. *J. Appl. Phys.* **2009**, *105* (12), 124314.

(9) Lu, K.-C.; Wu, W.-W.; Ouyang, H.; Lin, Y.-C.; Huang, Y.; Wang, C.-W.; Wu, Z.-W.; Huang, C.-W.; Chen, L. J.; Tu, K. N. The Influence of Surface Oxide on the Growth of Metal/Semiconductor Nanowires. *Nano Lett.* **2011**, *11* (7), 2753−2758.

(10) Mongillo, M.; Spathis, P.; Katsaros, G.; Gentile, P.; Sanquer, M.; De Franceschi, S. Joule-Assisted Silicidation for Short-Channel Silicon Nanowire Devices. *ACS Nano* **2011**, *5* (9), 7117−7123.
(11) Tang, W.; Dayeh, S. A.; Picraux, S. T.; Huang, J. Y.; Tu, K.-N. Ultrashort Channel Silicon Nanowire Transistors with Nickel Silicide Source/Drain Contacts. *Nano Lett.* **2012**, *12* (8), 3979−3985.
(12) van Gurp, G. J. Diffusion-limited Si Precipitation in Evaporated Al/Si Films. *J. Appl. Phys.* **1973**, *44* (5), 2040−2050.
(13) Liu, Z.; Wang, M.; Weng, Y.; Song, T.; Huo, Y.; Xie, J. Effect of Silicon on Grain Refinement of Aluminum Produced by Electrolysis. *Mater. Trans.* **2003**, *44* (10), 2157−2162.
(14) Mgbenu, E. N. Accelerated Aging of Al/Ge and Al/Si Thin Film Couples. *Thin Solid Films* **1980**, *65* (3), 267−274.
(15) Luong, M. A.; Robin, E.; Pauc, N.; Gentile, P.; Sistani, M.; Lugstein, A.; Spies, M.; Fernandez, B.; Den Hertog, M. I. In-Situ Transmission Electron Microscopy Imaging of Aluminum Diffusion in Germanium Nanowires for the Fabrication of Sub-10 Nm Ge Quantum Disks. *ACS Appl. Nano Mater.* **2020**, *3*, 1891.
(16) Luong, M. A. Investigation of Al Thermal Diffusion in Ge and SixGe1-x Alloy Nanowires Using in-Situ Transmission Electron Microscopy. PhD Thesis, Université Grenoble Alpes, 2019.
(17) El Hajraoui, K.; Luong, M. A.; Robin, E.; Brunbauer, F.; Zeiner, C.; Lugstein, A.; Gentile, P.; Rouvière, J.-L.; Den Hertog, M. In Situ Transmission Electron Microscopy Analysis of Aluminum−Germanium Nanowire Solid-State Reaction. *Nano Lett.* **2019**, *19* (5), 2897−2904.
(18) Sistani, M.; Luong, M. A.; den Hertog, M. I.; Robin, E.; Spies, M.; Fernandez, B.; Yao, J.; Bertagnolli, E.; Lugstein, A. Monolithic Axial and Radial Metal−Semiconductor Nanowire Heterostructures. *Nano Lett.* **2018**, *18* (12), 7692−7697.
(19) Hÿtch, M. J.; Snoeck, E.; Kilaas, R. Quantitative Measurement of Displacement and Strain Fields from HREM Micrographs. *Ultramicroscopy* **1998**, *74* (3), 131−146.
(20) Rouvière, J. L.; Sarigiannidou, E. Theoretical Discussions on the Geometrical Phase Analysis. *Ultramicroscopy* **2005**, *106* (1), 1−17.
(21) Rueda-Fonseca, P.; Robin, E.; Bellet-Amalric, E.; Lopez-Haro, M.; Den Hertog, M.; Genuist, Y.; André, R.; Artioli, A.; Tatarenko, S.; Ferrand, D.; Cibert, J. Quantitative Reconstructions of 3D Chemical Nanostructures in Nanowires. *Nano Lett.* **2016**, *16* (3), 1637−1642.
(22) Noé, P.; Vallée, C.; Hippert, F.; Fillot, F.; Raty, J.-Y. Phase-Change Materials for Non-Volatile Memory Devices: From Technological Challenges to Materials Science Issues. *Semicond. Sci. Technol.* **2018**, *33* (1), 013002.
(23) Guo, P.; Sarangan, A.; Agha, I. A Review of Germanium-Antimony-Telluride Phase Change Materials for Non-Volatile Memories and Optical Modulators. *Appl. Sci.* **2019**, *9* (3), 530.
(24) Yang, L.; Watling, J. R.; Wilkins, R. C. W.; Boriçi, M.; Barker, J. R.; Asenov, A.; Roy, S. Si/SiGe Heterostructure Parameters for Device Simulations. *Semicond. Sci. Technol.* **2004**, *19* (10), 1174−1182.
(25) Zeller, J. W.; Puri, Y. R.; Sood, A. K.; McMahon, S.; Efsthadiatis, H.; Haldar, P.; Dhar, N. K. *Design and Development of SiGe Based Near-Infrared Photodetectors*; LeVan, P. D., Sood, A. K., Wijewarnasuriya, P., D'Souza, A. I., Eds.; San Diego, CA, 2014.
(26) Majumder, K.; Das, N. R. Effects of Alloy Composition on Gain and Bandwidth of Si/SiGe and Si/GeSn Avalanche Photodiodes. *Optik* **2016**, *127* (5), 3059−3064.
(27) Brunbauer, F. M.; Bertagnolli, E.; Majer, J.; Lugstein, A. Electrical Transport Properties of Single-Crystal Al Nanowires. *Nanotechnology* **2016**, *27* (38), 385704.
(28) Ielmini, D.; Lacaita, A. L. Phase Change Materials in Non-Volatile Storage. *Mater. Today* **2011**, *14* (12), 600−607.
(29) Lee, B.-S.; Abelson, J. R.; Bishop, S. G.; Kang, D.-H.; Cheong, B.; Kim, K.-B. Investigation of the Optical and Electronic Properties of $Ge_2Sb_2Te_5$ Phase Change Material in Its Amorphous, Cubic, and Hexagonal Phases. *J. Appl. Phys.* **2005**, *97* (9), 093509.
(30) Lyeo, H.-K.; Cahill, D. G.; Lee, B.-S.; Abelson, J. R.; Kwon, M.-H.; Kim, K.-B.; Bishop, S. G.; Cheong, B. Thermal Conductivity of Phase-Change Material $Ge_2Sb_2Te_5$. *Appl. Phys. Lett.* **2006**, *89* (15), 151904.
(31) Song, H.; Hellawell, A. Solidification in the System Al-Ge-Si: The Phase Diagram, Coring Patterns, Eutectic Growth, and Modification. *Metall. Trans. A* **1990**, *21* (2), 733−740.
(32) Shankar, S.; Riddle, Y. W.; Makhlouf, M. M. Eutectic Solidification of Aluminum-Silicon Alloys. *Metall. Mater. Trans. A* **2004**, *35* (9), 3038−3043.
(33) Stefanescu, D. M.; Ruxanda, R. Solidification Structure of Aluminum Alloys, 2004.
(34) Ogata, K.; Sutter, E.; Zhu, X.; Hofmann, S. Ni-Silicide Growth Kinetics in Si and Si/SiO_2 Core/Shell Nanowires. *Nanotechnology* **2011**, *22* (36), 365305.
(35) Dellas, N. S.; Minassian, S.; Redwing, J. M.; Mohney, S. E. Formation of Nickel Germanide Contacts to Ge Nanowires. *Appl. Phys. Lett.* **2010**, *97* (26), 263116.
(36) Burchhart, T.; Lugstein, A.; Hyun, Y. J.; Hochleitner, G.; Bertagnolli, E. Atomic Scale Alignment of Copper-Germanide Contacts for Ge Nanowire Metal Oxide Field Effect Transistors. *Nano Lett.* **2009**, *9* (11), 3739−3742.
(37) El hajraoui, K.; Robin, E.; Zeiner, C.; Lugstein, A.; Kodjikian, S.; Rouvière, J.-L.; Den Hertog, M. In Situ Transmission Electron Microscopy Analysis of Copper−Germanium Nanowire Solid-State Reaction. *Nano Lett.* **2019**, *19* (12), 8365−8371.
(38) Liu, B.; Wang, Y.; Dilts, S.; Mayer, T. S.; Mohney, S. E. Silicidation of Silicon Nanowires by Platinum. *Nano Lett.* **2007**, *7* (3), 818−824.
(39) Kral, S.; Zeiner, C.; Stöger-Pollach, M.; Bertagnolli, E.; den Hertog, M. I.; Lopez-Haro, M.; Robin, E.; El Hajraoui, K.; Lugstein, A. Abrupt Schottky Junctions in Al/Ge Nanowire Heterostructures. *Nano Lett.* **2015**, *15* (7), 4783−4787.
(40) *Comprehensive Handbook of Chemical Bond Energies*; Taylor & Francis Group:https://www.taylorfrancis.com/books/9780429128684 (accessed Jan 9, 2020).
(41) Chou, Y.-C.; Wu, W.-W.; Cheng, S.-L.; Yoo, B.-Y.; Myung, N.; Chen, L. J.; Tu, K. N. In-Situ TEM Observation of Repeating Events of Nucleation in Epitaxial Growth of Nano $CoSi_2$ in Nanowires of Si. *Nano Lett.* **2008**, *8* (8), 2194−2199.
(42) Paul, D. J. Si/SiGe Heterostructures: From Material and Physics to Devices and Circuits. *Semicond. Sci. Technol.* **2004**, *19* (10), R75−R108.
(43) Stern, A. G. Design of High Quantum Efficiency and High Resolution, Si/SiGe Avalanche Photodiode Focal Plane Arrays Using Novel, Back-Illuminated, Silicon-on-Sapphire Substrates. In *Photodiodes - World Activities in 2011*; Park, J. W., Ed.; InTech: 2011.
(44) *Wildfire Nano-Chip*; DENSsolutions. https://Denssolutions.Com/Products/Wildfire/Nano-Chip/ (accessed Jan 9, 2020).
(45) Spies, M.; Sadre Momtaz, Z.; Lähnemann, J.; Anh Luong, M.; Fernandez, B.; Fournier, T.; Monroy, E.; I den Hertog, M. Correlated and In-Situ Electrical Transmission Electron Microscopy Studies and Related Membrane-Chip Fabrication. *Nanotechnology* **2020**, *31* (47), 472001.
(46) Jipelec™ Jetfirst: Compact & Robust RTP Furnace. ECM-USA, Industrial Furnace Manufacturer. http://www.Ecm-Usa.Com/Products/Rtp-Furnaces/Jetfirst (accessed Jan 9, 2020).

https://dx.doi.org/10.1021/acsanm.0c02303
ACS Appl. Nano Mater. 2020, 3, 10427−10436